International Journal of Advanced Technology in Engineering and Science
Vol. No.5, Issue No. 07, July 2017
www.ijates.com
ijates
ISSN 2348 - 7550

Microcontroller Based Optimization of Current-Fed Dual Active Bridge DC-DC Converter for PV Application

Mr. Shinde K.K[1], Mr. Wagh H.B[2]

[1]*Student of Electrical Engg Department, R.H. Sapat College, Nashik/ Pune University (India)*

[2]*Lecturer of Electrical Engineering Department, R.H. Sapat College, Nasik/ Pune University (India)*

ABSTRACT

This paper presents a thorough study of single-phase grid connected photovoltaic (PV) converter based on current-fed dual active bridge (CF-DAB) dc-dc converter. In this current-fed dual active full bridge dc-dc converter over the whole operating range under phase-shift and duty cycle control is introduced. An optimized operating mode achieving minimum root-mean square (rms) transformer primary current is derived in this paper under soft-switching conditions. The analysis and experimental results show that operating mode one and two has less power loss at higher output power range. With the proposed control, zero-voltage switching (ZVS) can be achieved for all switches within wide load range with low circulation loss. The converter with the proposed control has lower current ripples, circulation loss and peak current. Since current-fed DAB converters can be extended to multi-port and multi-phase applications. The simulation results are shown in this paper and the effectiveness of the proposed converter are verified by the experimental hardware results of a 5KW prototype as in previous paper.

Index terms- current fed dual active bridge converter, optimized operation, photovoltaic (PV), root mean square (RMS), soft switching.

I. INTRODUCTION

In grid connected PV system, Two-stage PV converter with high gain dc-dc converter cascaded by inverter is most popular topology [1-2]. In this structure, the reliability and lifetime of the PV system is reduces due to the bulky electrolytic capacitors application [3]. Therefore, efforts have been devoted to reduce the dc-link capacitance [4-11]. However, LVS dc-link capacitor may suffer from large voltage variations, which may not only affect the control system but also result in low-frequency ripple energy propagating into the PV side and reduces the MPPT performance. Extra circuits such as a high frequency current-fed active power filter (APF) and passive filter are employed to buffer the low-frequency ripple energy, but increase the cost and complexity of the PV system [8-10]. Small dc capacitors have also been proposed for PV application in voltage-fed dual active bridge (VF-DAB) dc-dc converter [11]. Nevertheless, unsymmetrical duty cycle control leads to high current stress on power device as well as potential saturation issue of magnetic cores due to the large transformer.

This paper introduces a novel single-phase PV system based on CF-DAB dc-dc converter with small DC-link capacitor that can achieve minimized low-frequency ripple effect on MPPT without adding extra components. The zero-voltage-switching (ZVS) characteristics are particularly suitable for PV application in current-fed topology. In the proposed approach, by regulating duty cycle the input PV voltage is directly controlled,

therefore, the PV arrays are immune to low-frequency power fluctuation and an optimized MPPT is achieved. Because of an advanced phase-shift control, large voltage ripples are permitted in the dc-link and the dc voltage ripples between primary side and second side are symmetrical, which contributes to reduce the transformer peak current. Furthermore, the interleaved structure is also helpful to reduce the input power ripple. The PV converter can allow the film capacitor to replace the bulky electrolytic capacitor with the proposed technology.

II. PROPOSED CURRENT-FED DUAL ACTIVE BRIDGE BASED PV CONVERTER

Fig. 1 shows the proposed single-phase grid-connected PV converter based on the CF-DAB dc-dc converter.

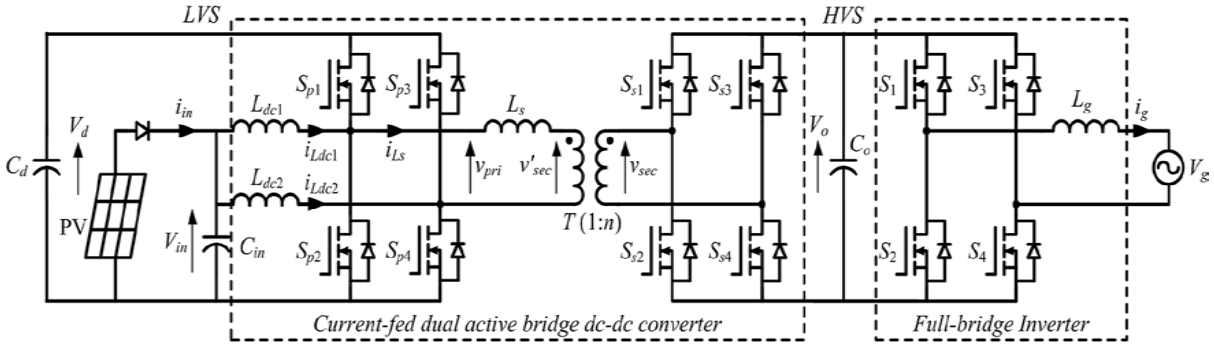

Fig-1. Proposed CF-DAB based PV converter.

The primary side of CF-DAB dc–dc converter performs the boosts operation and increase the PV voltage to a suitable level and provides galvanic isolation so that both the dc–dc converter and the inverter can operate efficiently. The leakage inductance of transformer Ls is as energy storage elements to transfer the power between two sides and the power flow is mainly controlled by a phase-shift angle φ. The middle points of two legs in LVS are connected to one energy source port through two DC inductors Ldc1-Ldc2, and duty cycle D is another control variable to adjust the power distribution between the two ports of LVS. Since the potential of efficiency improvement is limited for a traditional H-bridge inverter, the total efficiency of the PV converter largely depends on the optimized operation of the dc–dc stage.

III. OPERATING PRINCIPLE OF CF-DAB CONVERTER BASED PV APPLICATION

The proposed converter for CF-DAB converter for PV application is shown in fig-1. CF-DAB has two degrees of freedom, the duty cycle D and phase shift angle ϕ by which the PV voltage and LVS dc link voltage are controlled respectively. The primary side of the CF-DAB converter boost the PV voltage and directly performs the maximum power point tracking. On secondary side full bridge converter will co-ordinate with the CF-DAB converter to achieve the effective maximum power point tracking and delivered the maximum PV power and desired reactive power to the grid.

Fig-2. shows the operating sub areas of CF-DAB converter with positive power flow. In this the duty cycle D ranges between 0 to 1 and phase shift angle ϕ ranges from 0 to π. There are seven subareas that can be obtained from the four operating modes and each one has two conditions: D < 0.5 and D > 0.5. The phase shift angle less than $\frac{\pi}{2}$ and duty cycle arround 0.5 is preferred in order to reach high efficiency. Hence mode 1 and mode 2 are most common operating modes in CF-DAB converter. The waveforms of CF-DAB converter for different modes are shown in figure-3.

International Journal of Advanced Technology in Engineering and Science
Vol. No.5, Issue No. 07, July 2017
www.ijates.com
ijates
ISSN 2348 - 7550

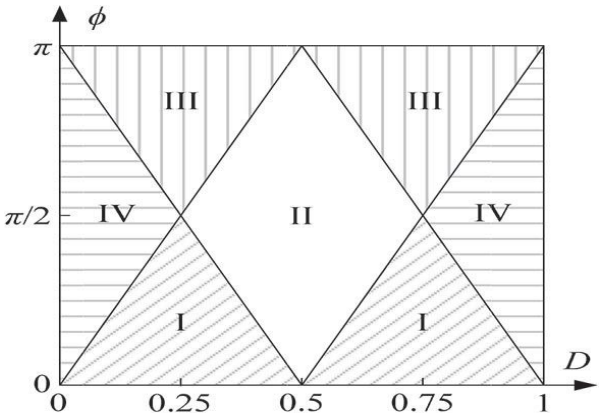

Fig-2. operating sub-areas of CF-DAB

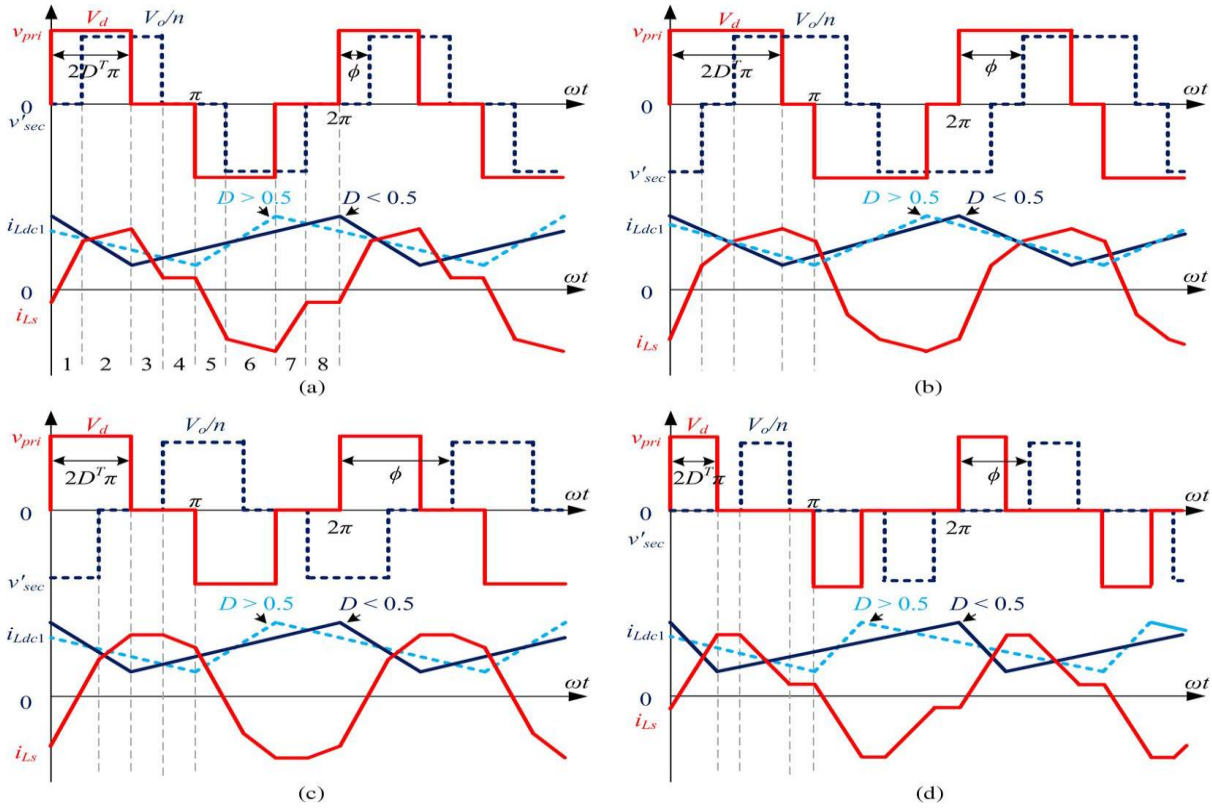

Fig-3. Waveforms of the CF-DAB converter. (a) Mode I: $0 < \varphi < \min\{2DT\pi, \pi - 2DT\pi\}$. (b) Mode II: $0.25 \leq DT \leq 0.5$, $2DT\pi \leq \varphi \leq \pi - 2DT\pi$. (c) Mode III: $\max\{2DT\pi, \pi - 2DT\pi\} < \varphi < \pi$. (d) Mode IV: $0 < DT < 0.25$, $2DT\pi \leq \varphi \leq \pi - 2DT\pi$. $DT = \min\{D, 1 - D\}$.

As shown in waveforms, V_{pri} and V'_{sec} are primery and primery refferd secondary side voltages respectively. i_{Ldc} is the dc inductor current and i_{Ls} is the transformer primery current. It can be seen that the transformer current is periodic and symmetrical over a switching cycle, hence the waveforms in half switching cycle are used for analysis.

The key waveforms of operating mode I are shown in Fig.3(a), where $0 < \varphi < \min\{2D^T\pi, \pi - 2D^T\pi\}$, and D^T is the minimum value of D and $1 - D$. Vpri and Vsec are the transformer primary-side voltage and the primary referred secondary-side voltage, respectively. i_{Ldc} is the dc inductor current, and i_{Ls} is the transformer primary

current. It can be observed that the transformer current is periodic and symmetrical over a switching cycle; hence, the waveforms in a half switching cycle are used for analysis. Over a half switching cycle the instantaneous current i_{Ls} (ωt) is represented as

$$i_{Ls}(\omega t) = \begin{cases} \left(\frac{Vd}{\omega Ls}\right)(\omega t - (1-d)D^T\pi), & 0 < \omega t \le \varphi \\ \left(\frac{Vd}{\omega Ls}\right)\left(d\varphi + (1-d)\left(\omega t - D^T\pi\right)\right), & \varphi < \omega t \le 2D^T\pi \\ \left(\frac{Vd}{\omega Ls}\right)(d(\varphi - \omega t) + (1+d)D^T\pi), & 2D^T\pi < \omega t \le 2D^T\pi + \varphi \\ \left(\frac{Vd}{\omega Ls}\right)(1-d)D^T\pi, & 2D^T\pi + \varphi < \omega t \le \pi \end{cases}$$

---------- (1)

where ω is the angular switching frequency, Ls is the leakage inductance, and d is the primary referred voltage ratio of the high-voltage side (HVS) dc link to the LVS dc link, i.e., d=Vo/nVd, with Vo and Vd being the HVS and LVS dc-link voltages, respectively, and η being the transformer turns ratio. Therefore, the transformer primary RMS current and peak current can be derived in the following:

$$Irms1=\sqrt{\frac{1}{\pi}\int_0^{\pi} iLs(\omega t)2d\omega t}$$

$$= \frac{Vd}{\omega Ls}\sqrt{\left(1-\frac{4}{3}D^T\right)[(1-d)D^T\pi]2 + \frac{d(6DT\pi-\varphi)\varphi 2}{3\pi}} \quad \text{---------- (2)}$$

$$Ipk1 = \begin{cases} iLs(2D^T\pi) = \frac{Vd}{\omega Ls[d\varphi + (1-d)DT\pi]}, & d \le 1 \\ iLs(\varphi) = Vd/\omega Ls[\varphi - (1-d)D^T\pi], & d > 1 \end{cases}$$

---------- (3)

The power flow equation is calculated by integrating the instant power over a half switching cycle as follows:

$$\int_0^{\pi} Vpri(\omega t).iLs(\omega t).d\omega t = \frac{Vd2}{\omega Ls}d\varphi\ (2D^2 - \frac{\varphi}{2\pi}) \quad \text{---------- (4)}$$

Where Vpri (ωt) is the primary-side voltage of the transformer, and i_{Ls} (ωt) is the primary-side transformer current. Similarly, the transformer RMS and peak currents, and the power flow equations for other operating modes can be derived, which are summarized in Table-1.

Table-1.

Mode	Throughout Power	Transformer Rms Current	Transformer Peak Current
1	$\frac{V_{d^2}}{\omega L_s}d\emptyset(2D^T - \frac{\emptyset}{2\pi})$	$\frac{V_d}{\omega L_s}\sqrt{\left(1-\frac{4}{3}D^T\right)[(1-d)D^T\pi]^2 + \frac{d(6D^T\pi-\emptyset)\emptyset^2}{3\pi}}$	$\begin{cases}\frac{V_d}{\omega L_s}[d\emptyset + (1-d)D^T\pi], d>1 \\ \frac{V_d}{\omega L_s}[\emptyset - (1-d)D^T\pi], d>1\end{cases}$
2	$\frac{V_{d^2}}{\omega L_s}d[\emptyset\left(1-\frac{\emptyset}{\pi}\right) - \frac{\pi}{2}(1-2D^T)^2]$	$\frac{V_d}{\omega L_s}\sqrt{\left(1-\frac{4}{3}D^T\right)[(1-d)D^T\pi]^2 + \frac{d\{(6D^T\pi-\emptyset)\emptyset^2 - [\emptyset-(1-2D^T)\pi]^3}{3\pi}}$	
3	$\frac{V_{d^2}}{\omega L_s} - d(\pi-\emptyset)[\frac{\emptyset}{2\pi} - (1-2D^T)$	$\frac{V_d}{\omega L_s}\sqrt{\left(1-\frac{4}{3}D^T\right)[(1-d)D^T\pi]^2 + \frac{d\{(3\emptyset-2D^T\pi)(2D^T\pi)^2)\,[\emptyset-(1-2D^T)\pi]^3\}}{3\pi}}$	$\frac{V_d}{\omega L_s}(1+d)D^T\pi$
4	$\frac{2V_{d^2}}{\omega L_s}d\pi(D^T)^2$	$\frac{V_d}{\omega L_s}\sqrt{\left(1-\frac{4}{3}D^T\right)[(1-d)D^T\pi]^2 + \frac{d\{(3\emptyset-2D^T\pi)(2D^T\pi)^2)\}}{3\pi}}$	

As the converter mainly operates in modes I and II, the minimized transformer peak current for a fixed dc-link voltage is achieved when the voltages on the LVS and the HVS are matched, i.e., d = 1. However, d = 1 will not minimize the RMS current. Since the ZVS technique is applied to the CF-DAB converter, the switching loss is greatly reduced, whereas the conduction loss becomes dominating in the device loss. Therefore, the RMS current is more critical than the peak current from the perspective of reducing power loss. To achieve a low power loss, the operating mode with a minimized RMS current is highly desired.

IV. SIMULATION

The simulink model for current fed dual active bridge dc-dc converter for PV application is shown in fig-4. The primary side of this converter is connected to the PV array and secondary side is connected to the grid system. It consists of high frequency transformer whose main function is to perform the boost operation and provides the galvanic isolation. The DC-DC converter that has high power capabilities comprised of eight semiconductor devices, a high frequency transformer, energy transfer inductor, and dc-link capacitors. Fig-5. Shows the Simulink model of pulse generator for CF-DAB converter for PV application. 5(a) and 5(b) shows pulse generator for H bridge DC-DC converter and 5(c) shows for inverter.

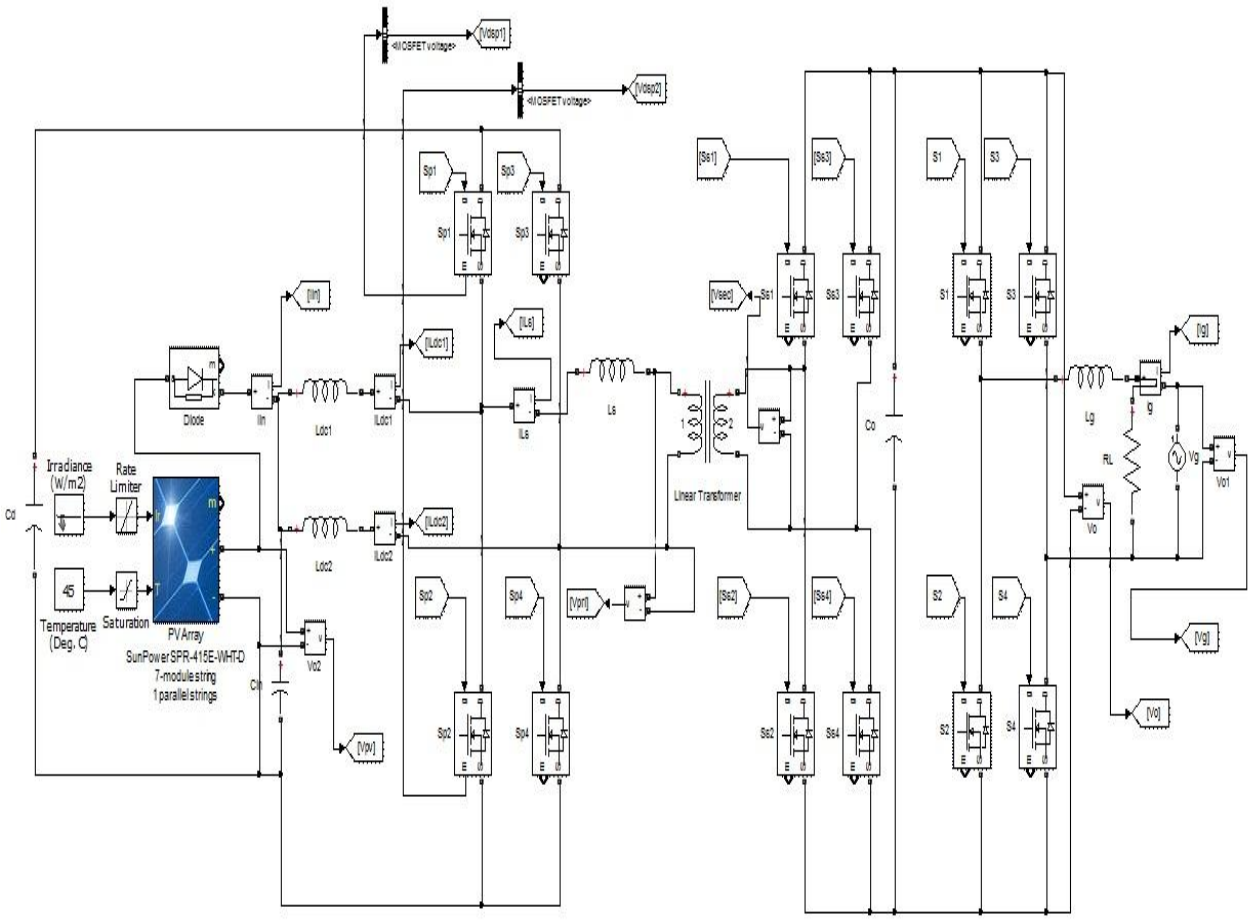

Fig-4. Simulink model for CF-DAB converter for PV application

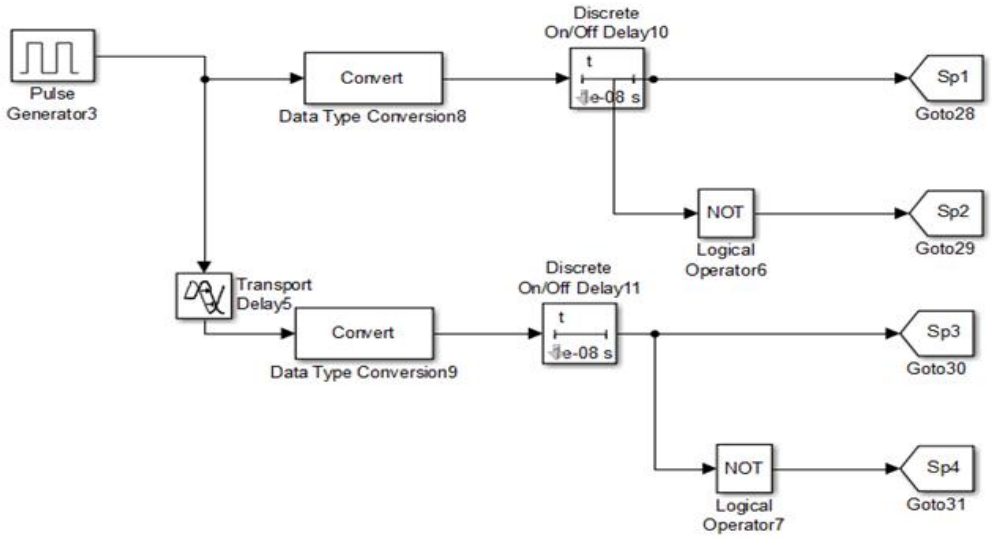

(a)

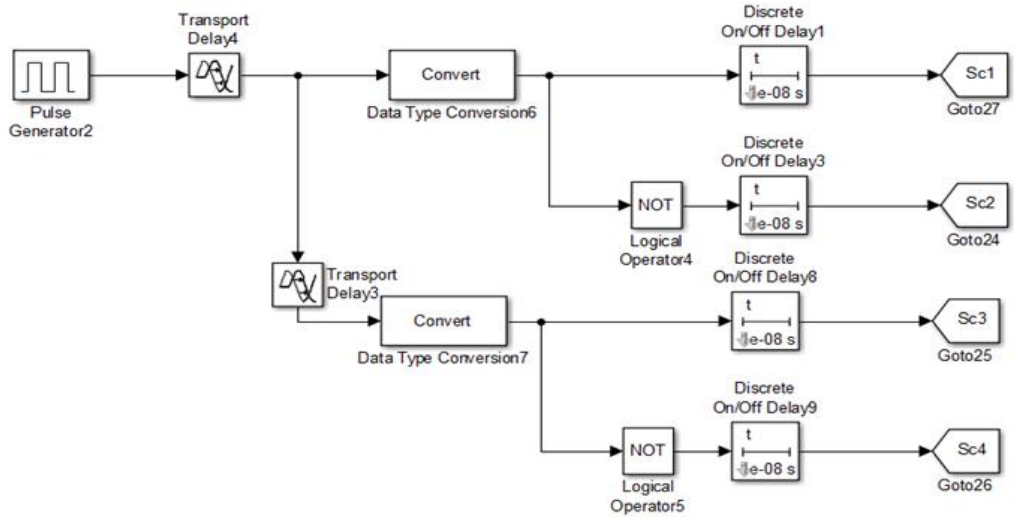

(b)

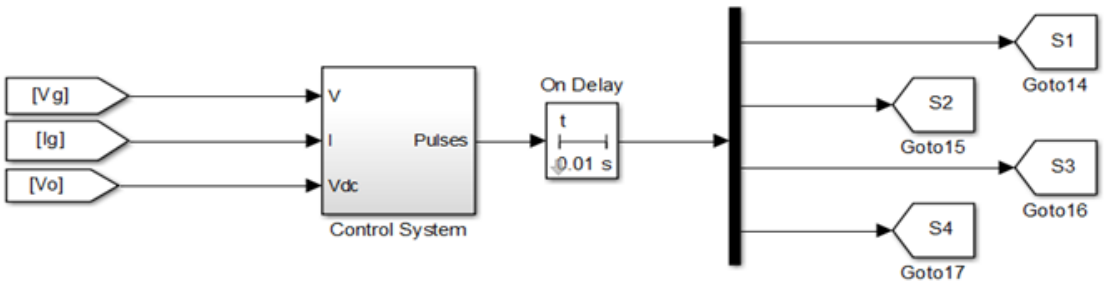

(c)

Fig-5. Simulink model of pulse generator for CF-DAB converter for PV application

International Journal of Advanced Technology in Engineering and Science
Vol. No.5, Issue No. 07, July 2017
www.ijates.com
ijates
ISSN 2348 - 7550

V. SIMULATION RESULTS

The simulation is shown in figure 4 and its results are shown in figure 5.As can be seen, the d = 1 mode in Fig. 5(a) has the minimum peak current, whereas its RMS current is much larger than that of the minimum-RMS-current mode (d = 0.875) in Fig. 5(b). Moreover, the lower switches in the primary side, i.e. Sp2 and Sp4, suffers from hard switching in the d = 1 mode, whereas soft switching is realized in the minimum-RMS current mode. At a high input voltage the minimum-RMS-current mode can extend the soft switching range. It should be noted that, the ZVS is not fully achieved for Sp2 in Fig. 5(b). This is because the analysis is based on an ideal model, without considering the parasitic capacitance and the power loss in the circuit. In a real case, to achieve the ZVS, the energy in the circuit must be sufficient to charge or discharge the output capacitance of the switches during the dead time. In Fig. 5(c), the ZVS of Sp2 is achieved when Vd is further increased. i.e., d = 0.845. The converter achieves the highest efficiency despite the increased peak and RMS currents over the minimum-RMS-current mode due to the ZVS turn on.

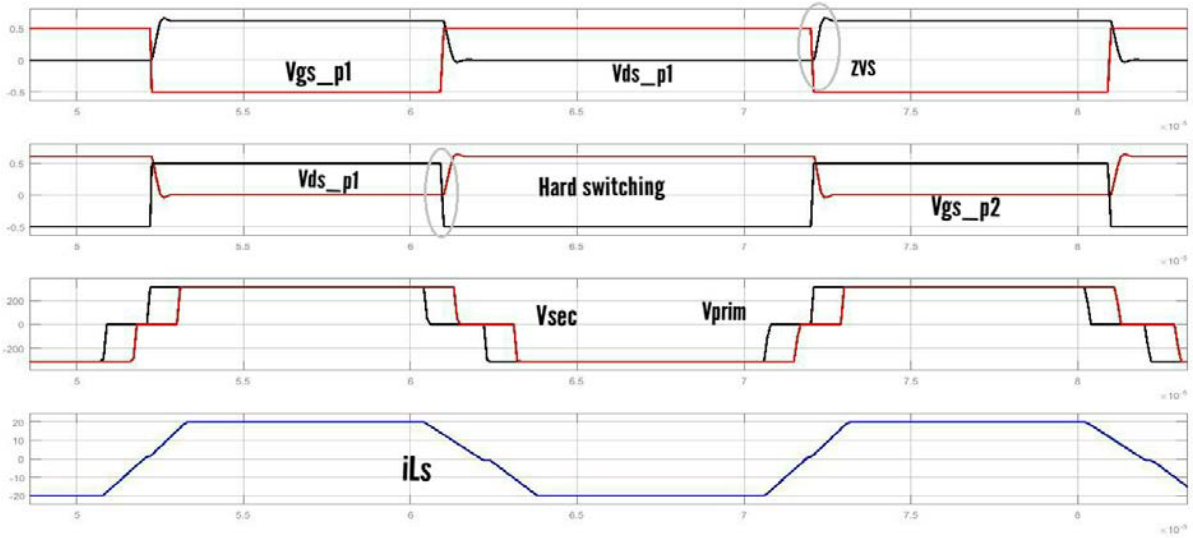

(a)

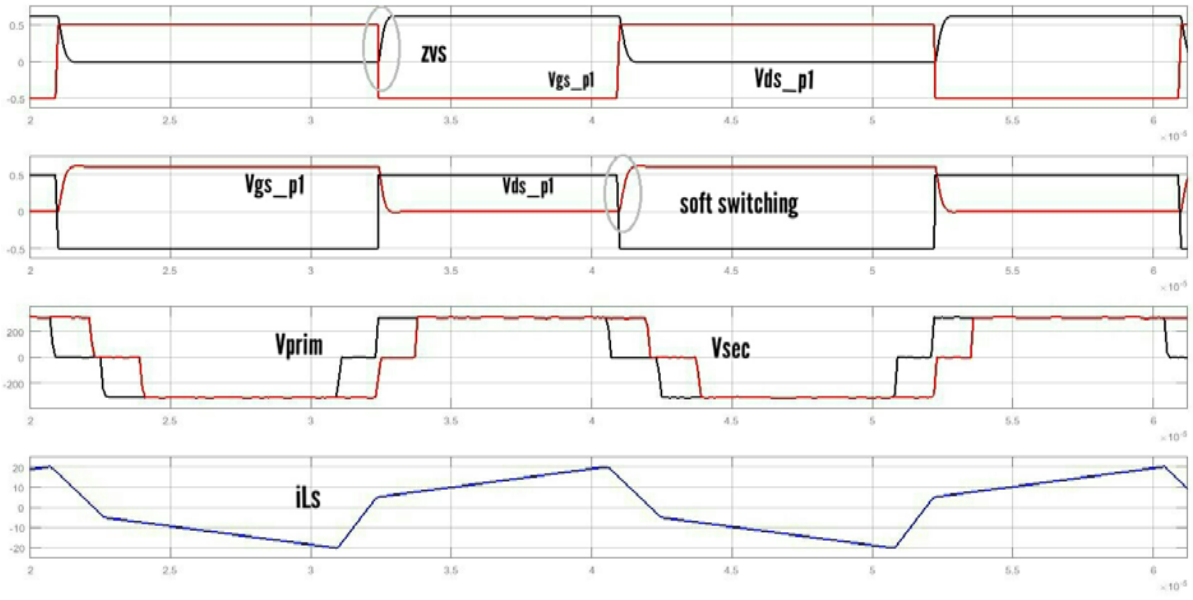

(b)

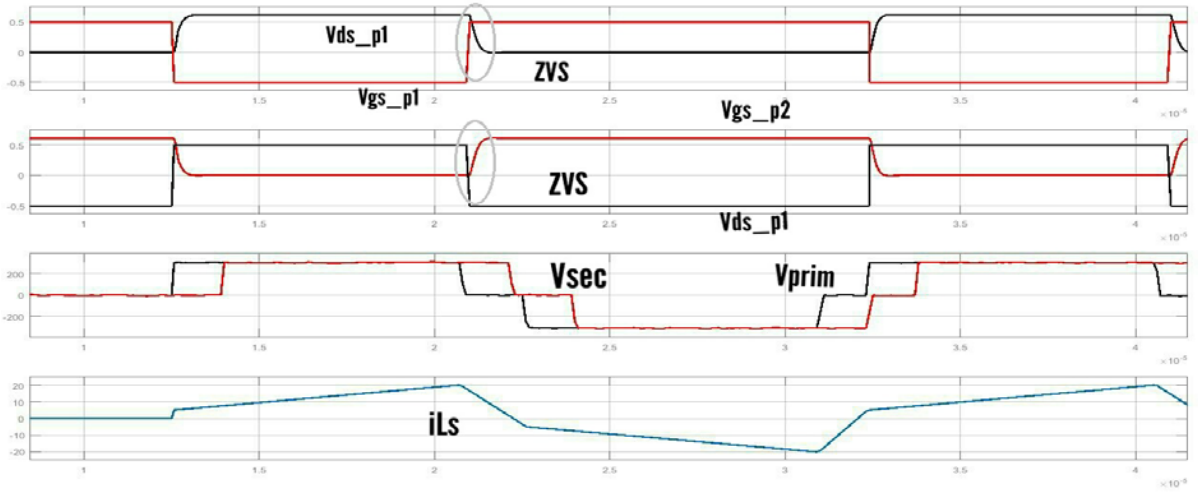

(c)

Fig-6. Experimental waveforms at *Vi*n = 200 V, *Vo* = 600 V, and *P* = 4 kW. (a) *d* = 1 mode at *Vd* = 307 V. (b) Minimum-RMS-current mode at *Vd* = 343 V. (c) Best efficiency operating at *Vd* = 355 V

VI. CONCLUSION

The current-fed full-bridge boost converter with zero voltage switching is simulated using matlab simulink and implemented using 16F8778 microcontroller. With proper selection of phase shift angle ϕ and duty cycle D, the current fed dual active bridge converter can achieve high efficiency. Seven sub areas that can be obtained by combining the four operating mode symmetrically, out of these modes, mode 1 and mode 2 is more suitable for CF-DAB converter operation. In addition soft switching conditions and minimum RMS current is also achieved. Further, efficiency can also be improved by using higher variable dc link voltage corresponding to the input voltage.

REFERENCE

[1] S.B.Kjaer, J.H.Pedersen, F. Blaabjerg. “A Review of Single-Phase Grid-connected Inverters for Photovoltaic Modules,” IEEE Trans. Industry Applica. Vol.41 no.5, pp.1292-1306, Sept. 2005.

[2] Q. Li and P. Wolfs "A review of the single phase photovoltaic module integrated converter topologies with three different dc link configurations", IEEE Trans. Power Electron., vol. 23, no. 3, pp.1320 -1333 2008.

[3] R. Margolis, "A review of PV converter technology cost and performance projections," NREL/SR 620-38771, 2006.

[4] Jin Xu, Sato, Y. , “An investigation of minimum DC-link capacitance in PWM rectifier-inverter systems considering control methods,” Energy Conversion Congress and Exposition (ECCE), 2012 IEEE, pp. 1071 - 1077.

[5] H. Hu , S. Harb , N. Kutkut , I. Batarseh and Z. John Shen "Power decoupling techniques for micro-inverters in PV systems-a review", Proc IEEE Energy Convers. Congr. Expo., pp.3235 -3240 P2010.

[6] X. Liu, H. Li and Z. Wang, “A fuel cell power conditioning system with low-frequency ripple free input current using a control-oriented power pulsation decoupling strategy”, early access, IEEE Trans. Power Electron., 2013

[7] X. Liu, H. Li and Z. Wang, "A new fuel cell power conditioning system with extended life time and minimized dc-bus capacitor", in Proc. Twenty-Eighth Annu. IEEE Appl. Power Electron. Conf. Exposition (APEC), Long Beach, CA, Mar. 2013, pp. 1926 – 1930.

[8] P. T. Krein , R. S. Balog and M. Mirjafari "Minimum energy and capacitance requirements for single-phase inverters and rectifiers using a ripple port", IEEE Trans. Power Electron., vol. 27, no. 11, pp.4690 -4698 2012.

[9] C. Kyritsis, N. P. Papanikolaou, and E. C. Tatakis, "A novel parallel active filter for current pulsation smoothing on single stage grid-connected AC-PV modules," in Proc. 12th EPE'07, Aalborg, Denmark, Sept. 2-5, 2007, pp. 1-10.

[10] Mirzahosseini, R., Tahami, F., "A lifetime improved single phase grid connected photovoltaic inverter," Power Electronics and Drive Systems Technology (PEDSTC), 2012 3rd, pp. 234-238.

[11] Z. Wang and H. Li "A soft switching three-phase current-fed bidirectional dc-dc converter with high efficiency over a wide input voltage range", IEEE Trans. Power Electron., vol. 27, no. 2, pp.669 -684 2012

[12] F. Z. Peng , H. Li , G. J. Su and J. S. Lawler "A new ZVS bidirectional dc-dc converter for fuel cell and battery application", IEEE Trans. Power Electron., vol. 19, no. 1, pp.54 -65 2004.

[13] Liming Liu, Yaosuo Xue, "A Coordinated Active and Reactive Power Control Strategy for Grid-Connected Cascaded Photovoltaic (PV) System in High Voltage High Power Applications," The Applied Power Electronics Conference and Exposition (APEC), 2013 IEEE.